

Article

Coupling DFIG-Based Wind Turbines with the Grid under Voltage Imbalance Conditions

Ahmed Sobhy^{1,2}, Ahmed G. Abo-Khalil^{3,4,*} , Dong Lei¹, Tareq Salameh³, Adel Merabet⁵ 
and Malek Alkasrawi⁶

- ¹ School of Automation, Beijing Institute of Technology, Beijing 100081, China; 3820170095@bit.edu.cn (A.S.); leidong@bit.edu.cn (D.L.)
- ² Department of Electrical Engineering, Faculty of Engineering, Port Said University, Port Said 42526, Egypt
- ³ Sustainable and Renewable Energy Engineering Department, College of Engineering, University of Sharjah, Sharjah P.O. Box 27272, United Arab Emirates; tsalameh@sharjah.ac.ae
- ⁴ Department of Electrical Engineering, College of Engineering, Assuit University, Assuit 71515, Egypt
- ⁵ Division of Engineering, Saint Mary's University, Halifax, NS B3H 3C3, Canada; adel.merabet@smu.ca
- ⁶ Industrial Assessment Center, University of Wisconsin-Milwaukee, Milwaukee, WI 53211, USA; alkasraw@uwp.edu
- * Correspondence: aabokhalil@sharjah.ac.ae

Abstract: A smooth coupling is implemented between the grid and doubly fed induction generator-based wind turbines (DFIG-WTs) during grid voltage imbalance. The nonlinear characteristics of a grid-connected DFIG-WT system may increase stresses on the mechanical and electrical components of wind turbines. Such difficulties are greatly increased during periods of voltage imbalance. Consequently, in this paper, a new control scheme is proposed to regulate DFIGs in order to support a smooth connection to the grid during voltage imbalance. In synchronization mode, the positive sequence of the rotor dq -axes currents regulates the stator q -axis EMF that is to be synchronized with the q -axis voltage of the grid-side voltage. The phase difference between the grid and stator voltages is compensated by adjusting the stator d -axis EMF to zero. Under normal conditions, a PR controller is used to dampen the negative sequence of the rotor dq -axes currents. PI current controllers are tuned to control the positive sequence of the DFIG rotor currents, while PR current controllers are used to regulate the negative sequence of the rotor currents during synchronization and under normal operation conditions. Experiments are performed to verify the smooth synchronization of the DFIG and the robustness of the proposed control scheme during grid voltage imbalance.

Keywords: doubly fed induction generator; synchronization; proportional resonant controller; grid voltage imbalance



Citation: Sobhy, A.; Abo-Khalil, A.G.; Lei, D.; Salameh, T.; Merabet, A.; Alkasrawi, M. Coupling DFIG-Based Wind Turbines with the Grid under Voltage Imbalance Conditions. *Sustainability* **2022**, *14*, 5076. <https://doi.org/10.3390/su14095076>

Academic Editor: Firoz Alam

Received: 8 March 2022

Accepted: 19 April 2022

Published: 23 April 2022

Publisher's Note: MDPI stays neutral with regard to jurisdictional claims in published maps and institutional affiliations.



Copyright: © 2022 by the authors. Licensee MDPI, Basel, Switzerland. This article is an open access article distributed under the terms and conditions of the Creative Commons Attribution (CC BY) license (<https://creativecommons.org/licenses/by/4.0/>).

1. Introduction

One of the major concerns of modern life is the issue of energy. Nowadays, power generation is primarily carried out by plants that use non-renewable resources as energy sources, which are mainly derived from fossil fuels. The limitation of reserves and the consequent increase in the price that is associated with fossil fuels point to the need to diversify energy sources. In addition, the environmental impact that is generated by the current scenario within the energy sector is considered high and needs to be continually rethought. The growing electricity demand, combined with the factors that were mentioned above, has motivated research into renewable sources that are environmentally friendly, which have low or no environmental impacts. Wind energy is a renewable alternative to the use of fossil fuels. This primary energy source is renewable and abundant in nature. The use of wind energy has high growth rates among renewable energy sources and is widely utilized worldwide [1]. The worldwide accumulated wind energy production has grown

to 743 GW by incorporating new projects of 93 GW in 2020, as reported by the global wind energy council, which is sufficient for generating 7% of the world's electricity demand [2].

In the wind turbine marketplace, the doubly fed induction generator (DFIG) is considered to be the most prevalent wind energy generation system. The DFIG rotor windings are connected to the grid through a back-to-back converter, which consists of the grid-side converter (GSC), DC-link capacitor, and the rotor-side converter (RSC), as shown in Figure 1. In the normal generation regime, the GSC is responsible for controlling the DC-link voltage and the reactive power that flows from that bus into the network. However, the RSC aims to control the stator's active and reactive power that passes into the grid [3]. A DFIG is characterized by a low converter capacity (only 30% of the generator rating). Additionally, the control of the two converters allows an excursion of the machine speed that is limited to $\pm 30\%$ of the nominal speed [4].

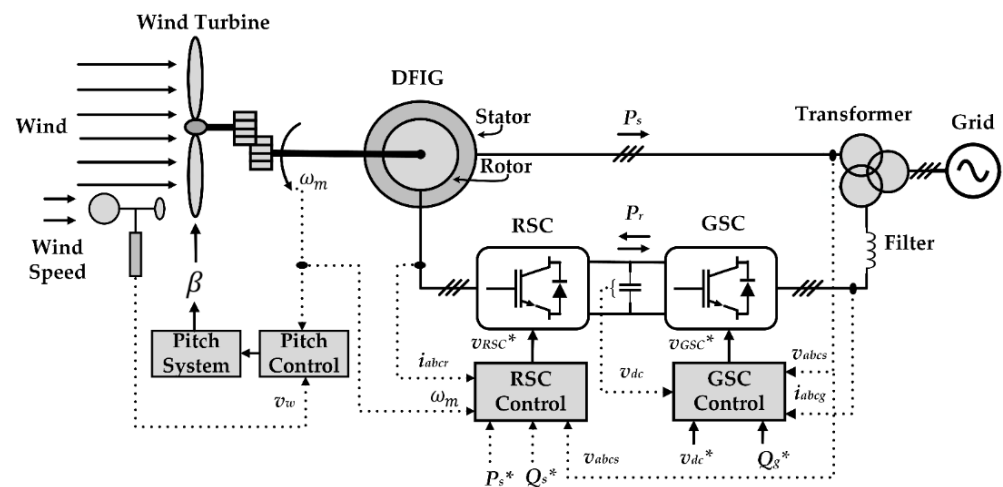


Figure 1. Block diagram of a grid-connected DFIG-based wind turbine.

The most common arrangement of the controllers for synchronization and the normal operation of a DFIG is composed of two loops with two proportional–integral (PI) cascading controllers. The outer loops control the active and reactive power of the stator during normal operation and the stator EMF during coupling with the grid, while the internal loops control the rotor currents. The controlled bidirectional slip power of a DFIG system makes it act as if it were a synchronous generator. Therefore, during the start-up process of a DFIG, the RSC aims to provide a smooth coupling between the stator windings and the grid [3]. Over the last decade, a limited number of publications have presented different control strategies for enhancing the coupling of DFIGs to the grid [5–12]. Vector control schemes with PI regulators have been commonly applied to achieve the synchronization of a DFIG and the grid [5,6]. However, these methods can affect the stability of the controlled DFIG or cause high-frequency oscillations. Recently, control schemes that were based on modern nonlinear controllers have been used for the enhancement of DFIG grid synchronization, in which the stator voltage of a DFIG was directly controlled to achieve a synchronization scheme that was based on sliding mode control (SMC) [7,8]. However, SMC suffers from the inadmissible chattering effect, which needs an additional control action to increase the robustness of the system. The model predictive control (MPC) of the DFIG rotor current has been employed to perform fast coupling to the grid [9]. Nevertheless, the main drawback of this technique is the necessary awareness of an accurate mathematical model of the rotor current. In [10,11], a robust grid synchronization scheme was proposed that involved applying a state feedback controller to both the RSC and GSC; however, this scheme is considered to be slightly complicated in application. The well-known fuzzy logic control (FLC) was also established for grid synchronization in [12]; however, the design and accuracy of the controller are dependent on the expertise of the user.

In addition, DFIGs are typically very susceptible to grid disturbances, such as a grid voltage imbalance due to the direct connection of DFIG stator windings to the electrical grid, which may affect the quality of the synchronization process. A voltage imbalance causes oscillating active and reactive power components, which are delivered to the electrical grid. Furthermore, a grid voltage imbalance produces a high amount of current imbalance within the DFIG rotor and stator windings due to the low impedance that is associated with the negative sequence components [13]. These currents are responsible for uneven heating in the windings of the machine and fluctuations in its electromagnetic torque. Nowadays, this is quite undesirable due to the continuous rise in the participation of wind energy in electrical power systems [14]. Several control techniques for DFIGs have been proposed in the scientific literature on the compensation of voltage imbalance. The existing strategies can be divided into two categories: hardware-based solutions and software-based solutions. Regarding hardware-based solutions, they either have low costs and simple structures but less reliability, such as crowbars and series dynamic braking resistors, or they have high reliability but higher costs and more complex structures, such as fault current limiters and DC choppers. However, software-based solutions can achieve a trade-off between complexity and reliability without additional costs [15].

Therefore, it is preferable to apply nonlinear controllers for the compensation of an imbalance in the grid-side voltage. These controllers can reduce the oscillations of the stator active power, reduce the DFIG electromagnetic torque oscillations, reduce stator current imbalance and reduce rotor current imbalance. Various control techniques have been proposed to minimize the four above-mentioned quantities under voltage imbalance conditions [16–28]. The use of four cascaded PI controllers to control the positive and negative sequence components of the rotor currents provides an acceptable performance when a system is running in a steady-state condition [16,17]. However, systems experience a slow response when DFIGs are running in transient conditions. Multivariable state feedback (MSF) controllers have been used to control the rotor current and allow it to perform better in transient conditions [18]. However, this scheme has a low transient response and low control accuracy due to the change in DFIG parameters. In [19], the direct torque control (DTC) technique was performed for DFIGs under symmetrical voltage dips. The DTC method offers the advantage of a fast response, but the issue of ripples remains the main challenge. Direct power control (DPC) has been used to reduce power and torque ripples during grid voltage imbalance [20–22]. However, due to the major effects of the active and reactive power oscillations and generator speed, the DPC method experiences the problem of unfixed switching frequency. A powerful nonlinear auto disturbance rejection control (ADRC) technology was proposed to fulfil the control requirements of a DFIG under grid voltage imbalance [23,24]. However, this framework employs an offline tuning method for the ADRC parameters that may be not suitable for changes in generator parameters that are caused by grid disturbances. SMC [25,26], MPC [27] and FLC [28] have also been implemented to control DFIGs during grid imbalance. Even though these controllers provide robust control performance when dealing with grid disturbances, they have some flaws that make their implementation more complex in practice. These drawbacks include the high control gains of the SMC method due to nonlinear compensation, the dependency on the generator parameters in the MPC method, and the possible control errors arising from not regularly updating the rules of the FLC method.

A proportional resonance (PR) controller has been used to regulate the negative sequence of the rotor currents, while PI controllers have been used to control the positive sequence [17,29–32]. This arrangement can eliminate the components of current imbalance from the rotor current by damping the resonant rotor current components at a frequency of 120 Hz. However, this arrangement has not yet been tested in the synchronization process. In this sense, the primary contributions of this article can be summarized as follows:

1. The positive sequence of the rotor current is controlled using PI controllers, while the negative sequence is controlled using proportional resonant (PR) controllers for both synchronization and operational modes;

2. The synchronization process of a DFIG starts when the generator speed reaches its minimum value. The positive and negative sequences of the q -axis stator EMF is regulated through the positive sequence of the dq -axes rotor current until the stator EMFs are equal to the grid voltages;
3. To compensate for the phase difference between the stator EMFs and the grid voltages, the d -axis stator EMFs are controlled to match the reference value of the d -axis grid voltages, which is equal to zero;
4. The stator EMF can be synchronized with the grid voltage by adding the calculated value of the compensation component to the slip angle;
5. Directly after the connection process, the average active and reactive power is adjusted by controlling the positive sequence of the rotor current. Meanwhile, the PR controllers are tuned at 120 Hz to regulate the negative sequence of the rotor current and attenuate the influence of the grid voltage imbalance on the DFIG's torque;
6. The effectiveness and robustness of the proposed control scheme for both synchronization and operational modes are proven experimentally during a grid imbalance.

2. Wind Turbine Modeling

A turbine's output power can be represented as:

$$P_t = \frac{1}{2} \rho \pi R^2 v^3 C_p(\beta, \lambda) \quad (1)$$

where P_t is the turbine's output power, ρ is the density of air, v is the wind speed through the turbine, and R is the radius of the turbine blades. The function $C_p(\beta, \lambda)$, which is given by Equations (2) and (3), represents the portion of wind energy that is collected by the wind turbine and is characterized as a power coefficient [33]:

$$C_p(\beta, \lambda) = C_1 \left(\frac{C_2}{\lambda_1} - C_3 \beta - C_4 \right) e^{-\frac{C_5}{\lambda_1}} + C_6 \lambda \quad (2)$$

$$\frac{1}{\lambda_1} = \frac{1}{\lambda - 0.08\beta} - \frac{0.035}{\beta^3 + 1} \quad (3)$$

The tip speed ratio is defined as:

$$\lambda = \frac{\omega_t R}{v} \quad (4)$$

where ω_t is the angular speed of the turbine rotor (rad/s).

The behavior of the $C_p(\beta, \lambda)$ function for various angles β and velocity relationships λ can be seen in Figure 2. During the normal operation of a wind turbine, the maximum power delivery is sought, which is a condition that, according to Equation (1), happens over the curve with the greatest gradient of the $C_p(\beta, \lambda)$ function. Equation (2) applies to all three-bladed turbines with parameters C_1 , C_2 , C_3 , C_4 , C_5 , and C_6 , which are determined using a regression approach [34].

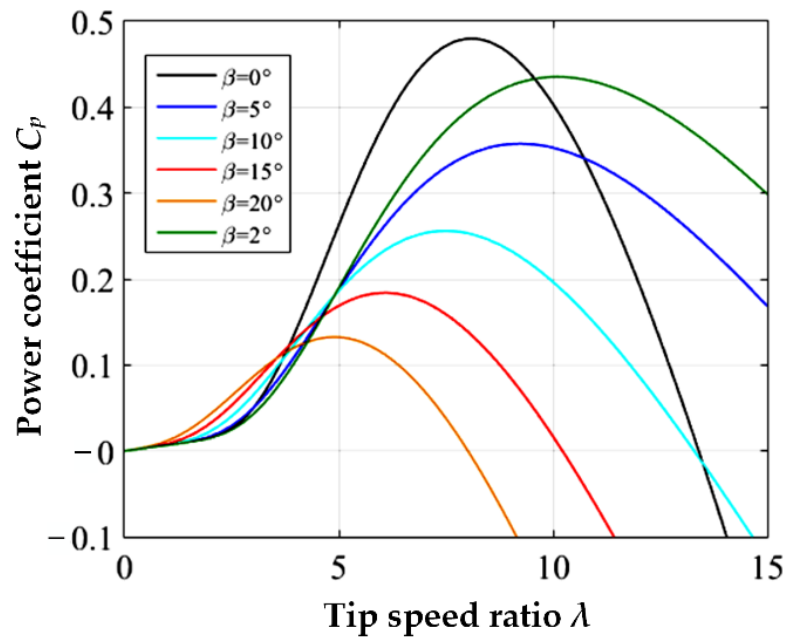


Figure 2. Variations in the power conversion coefficient as a function of pitch angle β .

3. DFIG Modeling

Using the DFIG $d-q$ equivalent circuit in Figure 3 [34], the voltage, current, and fluxes under stator flux-oriented control can be represented as [35]:

$$v_{ds} = R_s i_{ds} + \frac{d\lambda_{ds}}{dt} - \omega_e \lambda_{qs} \quad (5)$$

$$v_{qs} = R_s i_{qs} + \frac{d\lambda_{qs}}{dt} + \omega_e \lambda_{ds} \quad (6)$$

$$v_{dr} = R_r i_{dr} + \frac{d\lambda_{dr}}{dt} - \omega_{sl} \lambda_{qr} \quad (7)$$

$$v_{qr} = R_r i_{qr} + \frac{d\lambda_{qr}}{dt} + \omega_{sl} \lambda_{dr} \quad (8)$$

$$\lambda_{ds} = L_s i_{ds} + L_m i_{dr} \quad (9)$$

$$\lambda_{qs} = L_s i_{qs} + L_m i_{qr} \quad (10)$$

$$\lambda_{dr} = L_m i_{ds} + L_r i_{dr} \quad (11)$$

$$\lambda_{qr} = L_m i_{qs} + L_r i_{qr} \quad (12)$$

where R_s is the stator resistance, R_r is the rotor resistance, ω_e is the angular velocity, ω_{sl} is the slip angular velocity, v_{dqs} is the stator dq -axes voltages, v_{dqr} is the rotor dq -axes voltages, i_{dqs} is the stator dq -axes currents, λ_{dqs} is the stator dq -axes flux linkage, i_{dqr} is the rotor dq -axes currents, λ_{dqr} is the rotor dq -axes flux linkage, L_s is the stator inductance, L_r is the rotor inductance, and L_m is the magnetizing inductance.

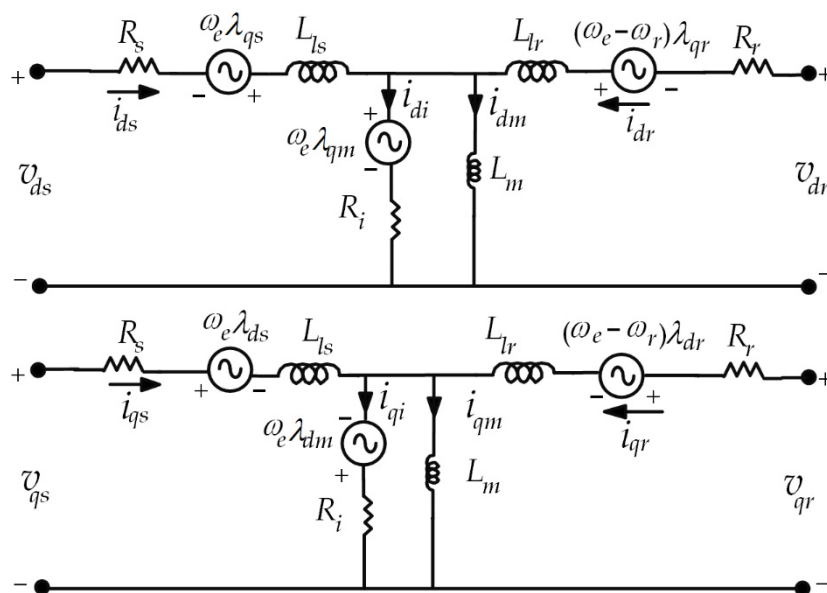


Figure 3. DFIG equivalent circuit in dq synchronous coordinates.

As shown in Figure 4 [34], the flux vector of the stator is aligned with the d-axis as follows:

$$\lambda_{ds} = \lambda_s, \lambda_{qs} = 0 \tag{13}$$

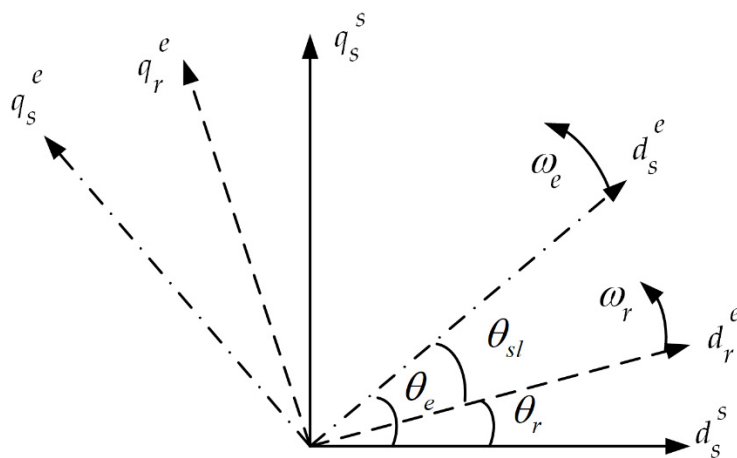


Figure 4. Diagram of the stator flux-oriented control vector.

The active and reactive power of the rotor and stator, as well as the electromagnetic torque that is produced by the DFIG, in the condition of invariant power can be calculated as [34]:

$$P_s = \frac{3}{2}(v_{qs}i_{qs} + v_{ds}i_{ds}) = -\frac{3}{2} \cdot \frac{L_m}{L_s} \cdot v_{qs}i_{qr} \tag{14}$$

$$Q_s = \frac{3}{2}(v_{qs}i_{ds} - v_{ds}i_{qs}) = \frac{3}{2} \cdot \frac{L_m}{L_s} \cdot v_{qs}(i_{ms} - i_{dr}) \tag{15}$$

$$T_e = \left(\frac{3}{2}\right) \left(\frac{P}{2}\right) (\lambda_{ds}i_{qs} - \lambda_{qs}i_{d}) \tag{16}$$

where P_s is the stator’s active power, Q_s is the stator’s reactive power, and T_e is the electromagnetic torque.

4. DFIGs under Grid Voltage Imbalance

The stator's voltages and active and reactive power during grid voltage imbalance can be stated as [36]:

$$v_{ds}^p = d \lambda_{ds}^p / dt + j\omega_e \lambda_{ds}^p \quad (17)$$

$$v_{qs}^p = d \lambda_{qs}^p / dt + j\omega_e \lambda_{qs}^p \quad (18)$$

$$P_s + jQ_s = -\frac{3}{2} \hat{v}_{qs}^p \hat{i}_{qs}^p \quad (19)$$

where $\hat{\cdot}$ is the superscript of the conjugated space vector, v_{dqs}^p is the positive components of the stator dq -axes voltages, i_{dqs}^p is the positive components of the stator dq -axes currents, and λ_{dqs}^p is the positive components of the stator dq -axes flux linkage.

During grid voltage imbalance, the instantaneous DFIG stator active and reactive power in (19) can be expressed as [37]:

$$P_s = P_{s0} + P_{ecos2} \cos(2\omega_e t) + P_{esin2} \sin(2\omega_e t) \quad (20)$$

$$Q_s = Q_{s0} + P_{ecos2} \cos(2\omega_e t) + P_{esin2} \sin(2\omega_e t) \quad (21)$$

where P_{s0} is the average component of the stator active power, Q_{s0} is the average component of the stator reactive power, P_{esin2} is the sin oscillating stator power component at twice the grid frequency, and P_{ecos2} is the cos oscillating stator power component at twice the grid frequency.

The positive sequence of the d -axis is aligned with the positive sequence of the stator voltage in stator voltage orientation, as illustrated in Figure 5, which implies that $v_{qs}^p = 0$. The dq -axes sequence of the stator voltage can be defined as [36]:

$$v_{dqs}^p = j\omega_e \lambda_{dqs}^p \quad (22)$$

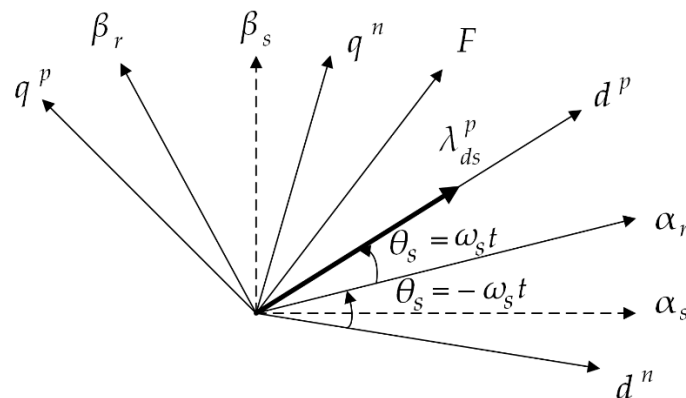


Figure 5. Transformation of vectors in the different reference frames.

Under grid voltage imbalance, the electromagnetic power of a DFIG is divided into its continuous elements and two pulsating parts as follows [13]:

$$P_e = P_{e0} + P_{ecos2} \cos(2\omega_e t) + P_{esin2} \sin(2\omega_e t) \quad (23)$$

The electromagnetic torque is given as follows:

$$T_e = p P_e / \omega_r \quad (24)$$

where ω_r is the rotor angular velocity.

Accordingly, the electromagnetic torque matrix during grid voltage imbalance can be expressed as [13]:

$$\begin{bmatrix} T_{e0} \\ T_{ecos2} \\ T_{esin2} \end{bmatrix} = -\frac{3p_n L_m}{2\omega_e L_s} \begin{bmatrix} -v_{ds}^p & -v_{qs}^p & v_{ds}^n & v_{qs}^n \\ v_{qs}^n & -v_{ds}^n & v_{qs}^p & -v_{ds}^p \\ v_{ds}^n & v_{qs}^n & -v_{ds}^p & -v_{qs}^p \end{bmatrix} \begin{bmatrix} i_{dr}^p \\ i_{qr}^p \\ i_{dr}^n \\ i_{qr}^n \end{bmatrix} \quad (25)$$

where T_{e0} is the average component of the electromagnetic torque, T_{esin2} is the sin oscillating torque component at twice the grid frequency, T_{ecos2} is the cos oscillating torque component at twice the grid frequency, i_{dqr}^p is the positive rotor components of the dq -axes currents, and i_{dqr}^n is the negative rotor components of the dq -axes currents.

The dq -axes negative reference components of a DFIG rotor can be calculated by eliminating the torque ripple components T_{ecos2} and T_{esin2} in Equation (25), such that [13]:

$$\begin{cases} i_{dr}^{n*} = \frac{1}{v_{sd}^p} (v_{ds}^n i_{dr}^p + v_{qs}^n i_{qr}^p) \\ i_{qr}^{n*} = \frac{1}{v_{sd}^p} (v_{ds}^n i_{qr}^p - v_{qs}^n i_{dr}^p) \end{cases} \quad (26)$$

where i_{dqr}^{n*} is the rotor negative components of the dq -axes currents.

The RSC controllers are implemented under grid voltage imbalance situations in the normal operating mode, as shown in Figure 6. In this system and when using two control loops, the currents in the rotor are controlled along the dq reference axes. The generator’s reactive and active power (or electromagnetic torque) are controlled by the dq -axes current loops. The bottom part of the block diagram shows the control of the negative sequence by controlling the 120-Hz torque components. The extraction of the positive and negative sequences of the dq -axes rotor is shown in Figure 7.

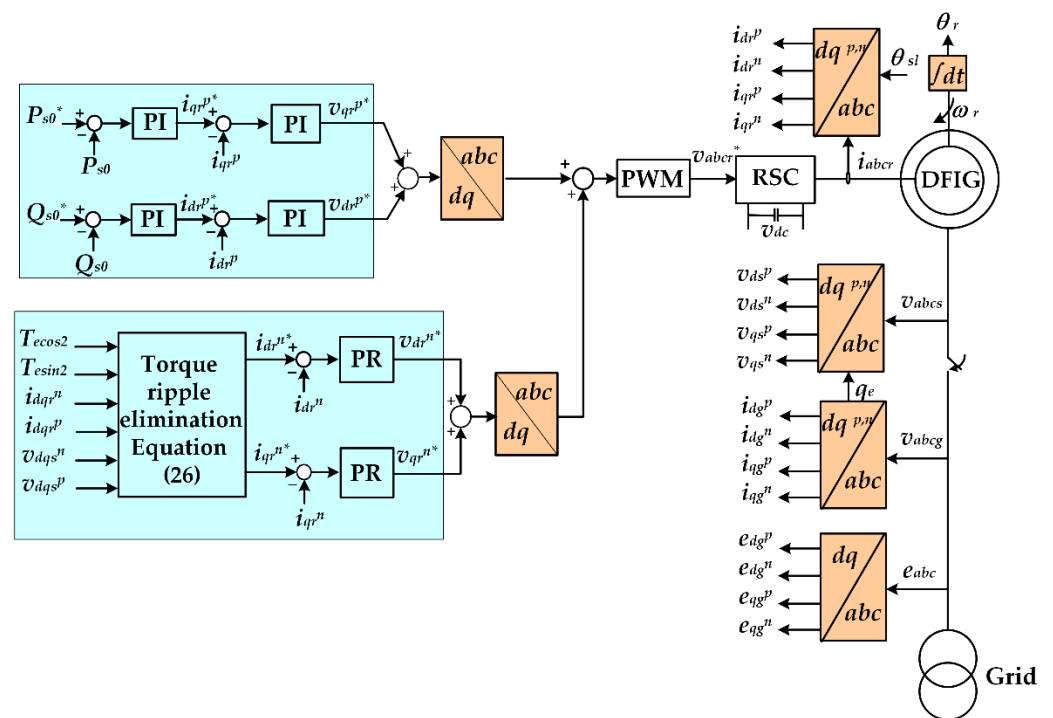


Figure 6. Diagram of DFIG rotor-side converter control during normal operation.

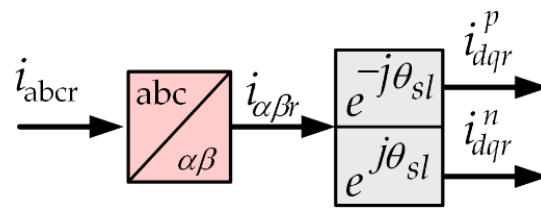


Figure 7. Extraction of rotor current components.

To obtain the proportional and integral gain of the PI controller for the internal current loop of the grid-side converter, the Naslin polynomial technique was used in this study [38]. The proportional gain K_p and the integral gain K_i for the positive dq -axes current controllers are listed in Table 1.

Table 1. PI controller gains.

PI Gains	K_p	K_i
Positive sequence controllers	3.64	123.55

5. Synchronization with the Grid

Initially, during the start-up process of the system, which is represented by Figure 8, switch S1 is open and the synchronization process starts when the generator speed reaches its minimum value. The grid voltages e_{abc} , the stator voltages v_{abc} , and the rotor currents i_{abcr} are obtained experimentally during the synchronization process. The positive and negative sequences of the q -axis stator EMF are regulated through the positive sequence of the dq -axes rotor current until the stator EMFs are equal to the grid voltages. The position θ_s is obtained by integrating the speed signal, which the PI controller permanently regulates in order to maintain the d -axis grid voltage at zero, as shown in Figure 9a. To compensate for the phase difference between the stator EMFs and grid voltages, the d -axis stator EMFs are controlled to match the reference value of the d -axis grid voltages, which is equal to zero. Figure 9b depicts the phase difference compensation process and provides the compensation component $\delta\theta_{sl}$. Therefore, the stator EMF can be synchronized with the grid voltage by adding the calculated value of $\delta\theta_{sl}$ to the slip angle. The synchronization is then concluded with the closing of the switch, which connects the machine's stator to the grid. Directly after the connection process, the DFIG control mode is changed from synchronization to operational mode. The average active and reactive power are regulated to follow their command targets and minimize the response of the voltage imbalance on the generator's torque. The synchronization sequence is depicted in the flowchart that is shown in Figure 10.

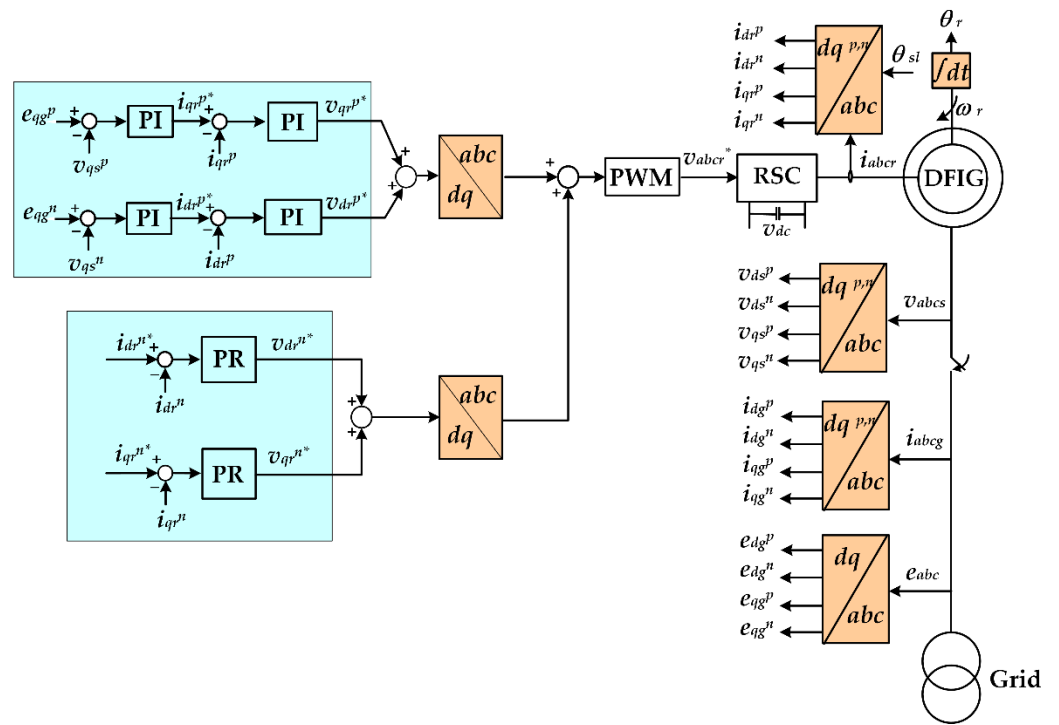


Figure 8. Diagram of DFIG rotor-side converter control during synchronization mode.

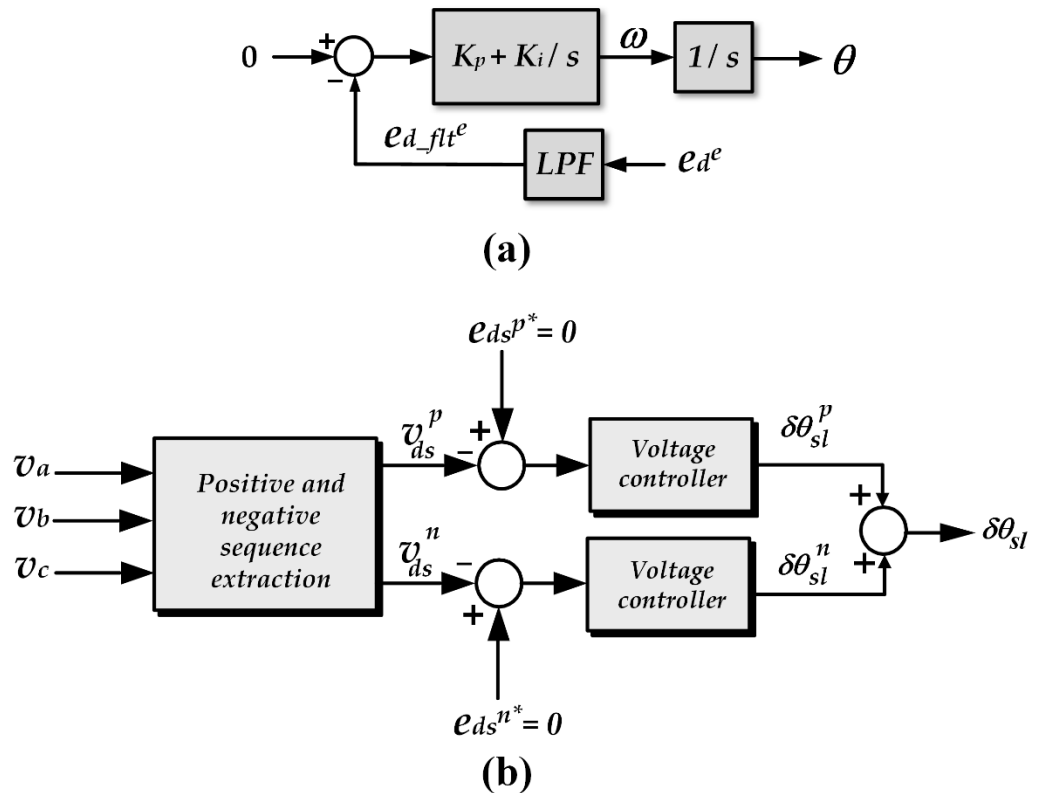


Figure 9. (a) Source angle detection; (b) phase difference compensation for synchronization.

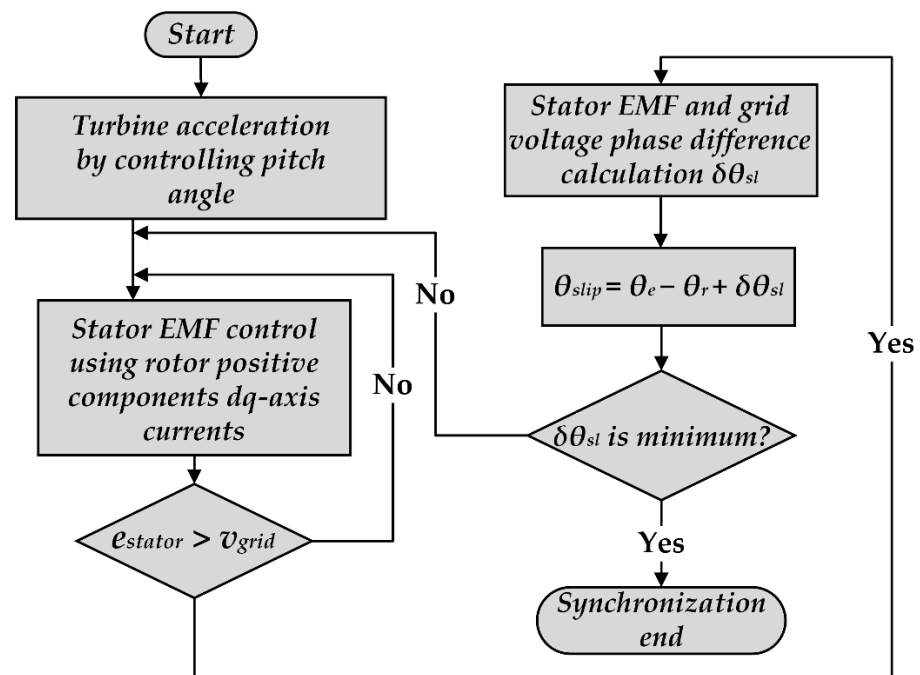


Figure 10. Synchronization steps.

6. Experimental Results and Discussion

This section presents the experimental results for a wind system that was based on the 3 kW DFIG from LabVolt and the wind turbine simulator from Labvolt, as shown in Figure 11. The DSP board, data acquisition board, and sensors were utilized, as well as the laboratory bench, to acquire the experimental results. The experimental results of the synchronization process between the stator and grid are shown during the system's start-up process. The DFIG rotor current dynamics are presented with the results that were obtained experimentally. The experimental results were based on a 10 kHz switching frequency, a 2200 μF DC bus capacitance, and a 100 μs sampling time. The DFIG and turbine simulator data are presented in Tables A1 and A2.

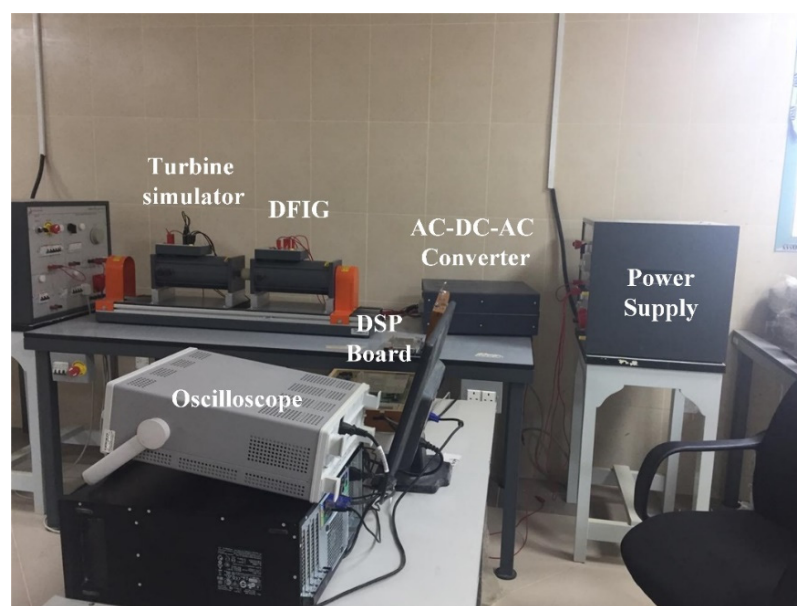


Figure 11. Experimental set-up of the DFIG system.

As depicted in Figure 12, the amplitudes of two phases of the 3-phase grid voltages were reduced to generate the grid voltage imbalance conditions.

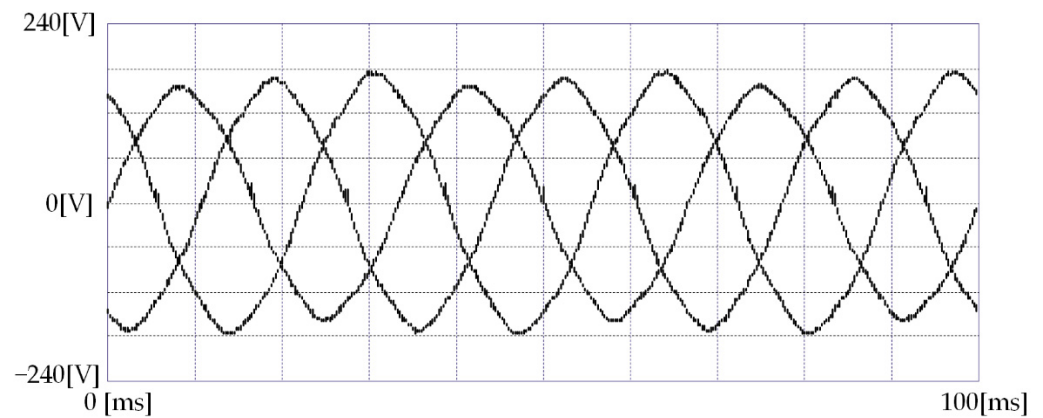


Figure 12. Three-phase grid voltage imbalance.

The stator voltage and grid voltage during the synchronization process are shown in Figure 13, which shows the start and end waveforms of the synchronization. The synchronization process was carried out in approximately 20 ms, which indicates that the synchronization process was achieved smoothly and without causing any disturbances in the grid voltage.

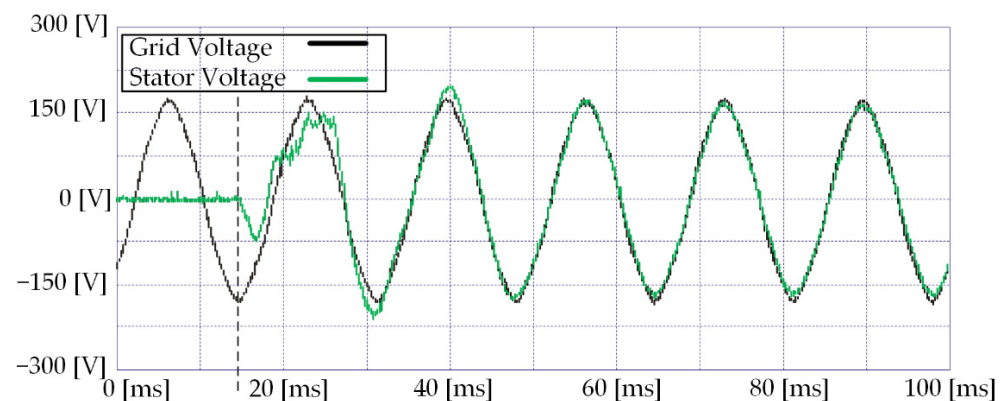


Figure 13. Synchronization of the DFIG stator with the grid.

After closing the switch, the reactive and active power controllers were activated to control the average values by regulating the positive sequence of the dq -axes rotor currents. When the negative sequence of the rotor currents was not controlled, the reactive and active power oscillated around the average values, which were 0 VAR and 1000 W, respectively. Figure 14a,b show the power oscillations around the average values with a frequency of 120 Hz, which represents the negative current sequence. After connecting to the grid, the stator reactive power oscillation amplitude was approximately 120 VAR. Similarly, the stator active power oscillation amplitude was about 100 W around the mean power.

Due to the existence of the 120 Hz components within the stator currents, the torque oscillated around the average value with an amplitude of 2 Nm when there was no control of the torque ripple, as illustrated in Figure 15a. When torque ripple control was applied, the amplitude of the ripple reduced to about 0.3 Nm, as shown in Figure 15b. The proposed controller was robust and minimized the torque ripple significantly.

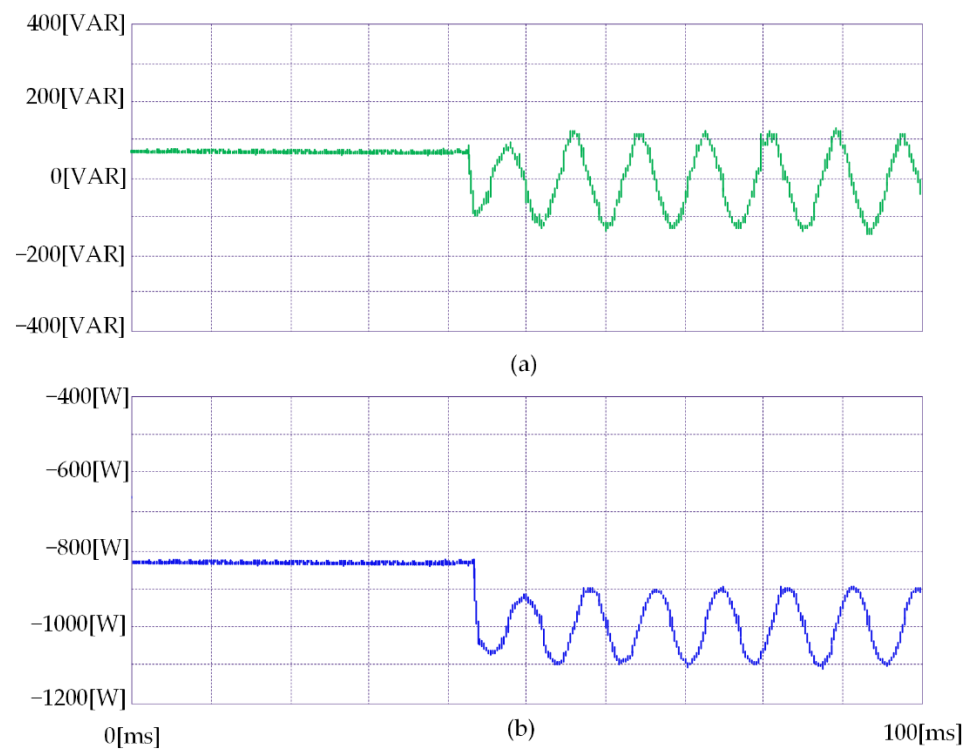


Figure 14. Stator (a) reactive power and (b) active power during the synchronization.

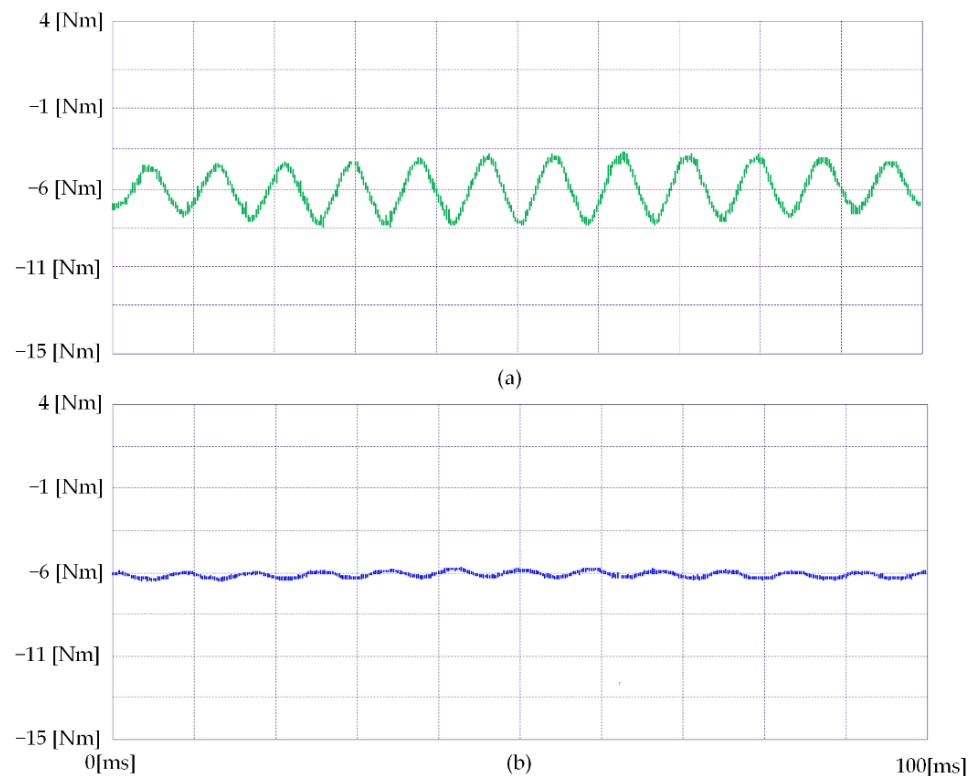


Figure 15. Generator torque (a) without torque ripple elimination control and (b) with torque ripple control.

Figure 16a shows the spectrum of the generator torque when using a conventional control method, while Figure 16b shows the spectrum when the proposed controller was used. The generator's 120 Hz torque oscillation component was reduced significantly. In comparison, the components 240 Hz and 360 Hz were canceled by regulating the negative

sequence of the rotor dq -axes currents, which reduced the mechanical stress on the turbine shaft. The harmonic spectrum of the stator dq -axes currents is illustrated in Figure 17. The double frequency component (120 Hz) was dominant, especially in the d -axis current. These components were eliminated and, consequently, the torque ripple decreased.

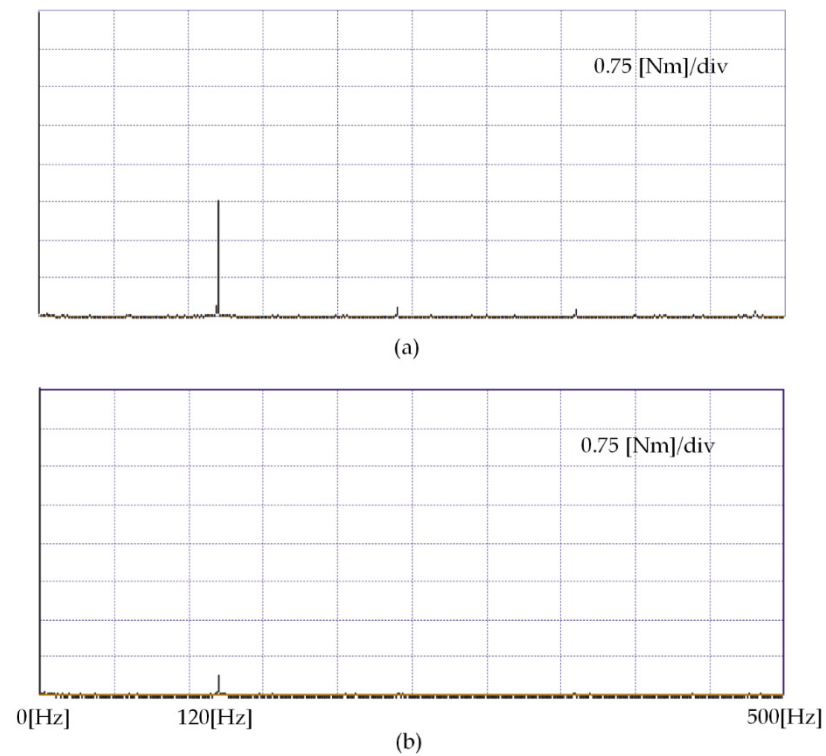


Figure 16. Torque ripple spectrum (a) without ripple control and (b) with ripple control.

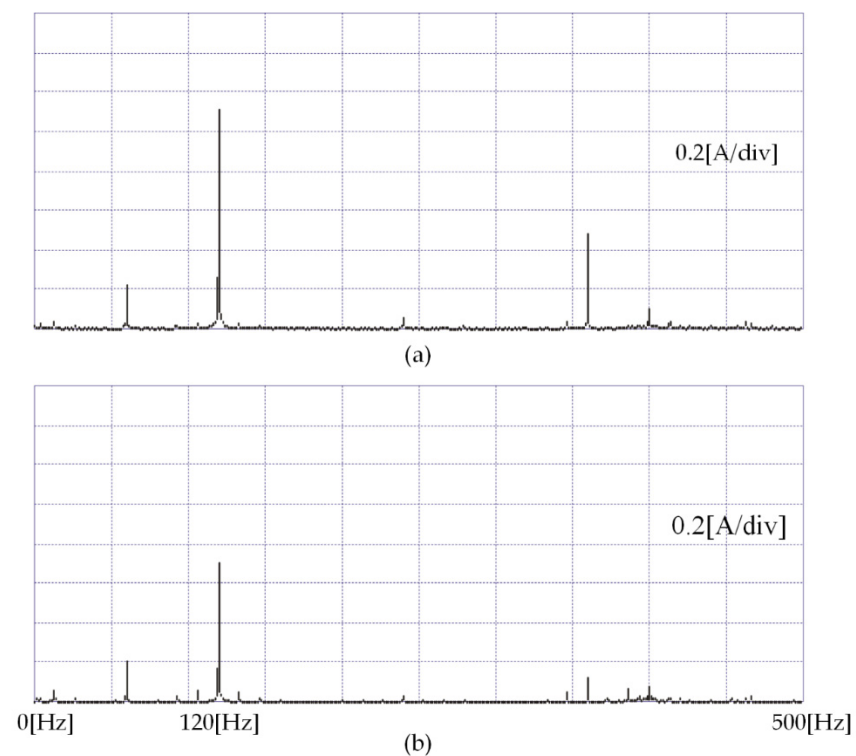


Figure 17. Harmonic spectrum of (a) stator d -axis current and (b) stator q -axis current.

When the conventional control method was utilized to regulate the stator's active and reactive power, both included the 120 Hz components, as illustrated in Figure 18a,b. The amplitude of the reactive power ripple was 120 VAR when the mean reactive power was controlled to be zero, as in Figure 18a. Similarly, the active power oscillated with an amplitude of 100 W, as in Figure 18b.

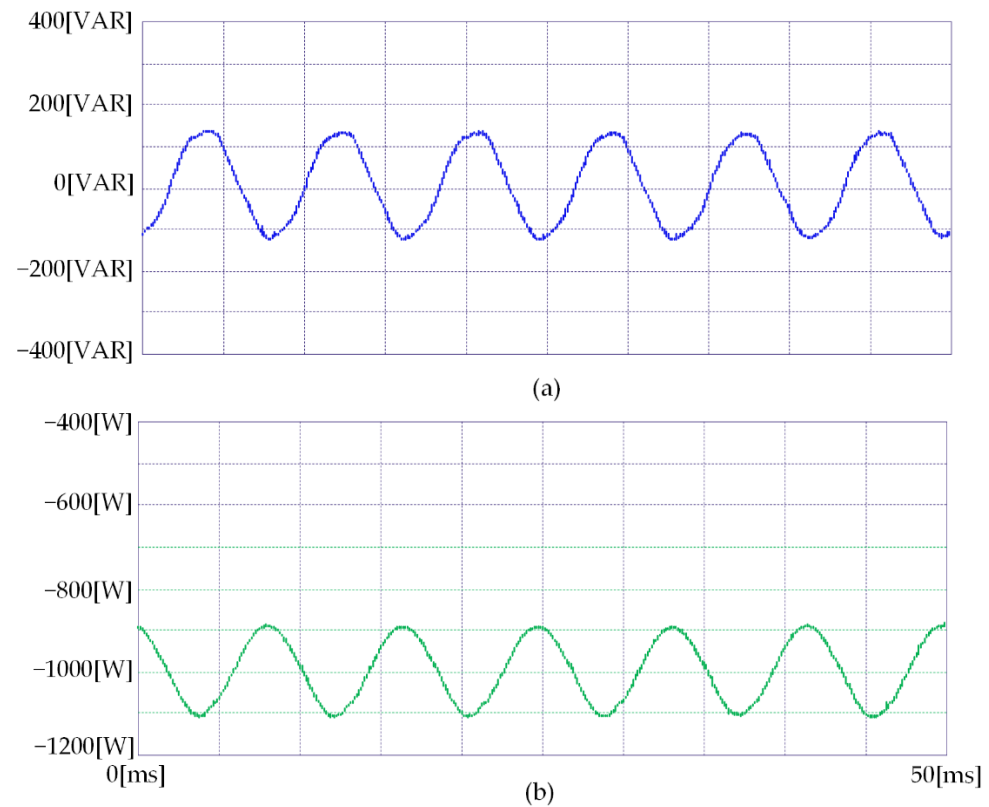


Figure 18. Steady-state stator (a) reactive power and (b) active power without torque ripple control.

The stator reactive power ripple was suppressed when the generator torque ripple was controlled, as illustrated in Figure 19a. However, controlling the torque ripple by regulating the negative sequence of the rotor current did not reduce the stator active power ripple, as seen in Figure 19b. This was because it is impossible to reduce both the stator active and reactive power ripples simultaneously.

Figure 20a,b show the grid voltage and current waveforms when the compensation technique for grid voltage imbalance was implemented. By controlling the negative component of the grid current, the ripple component of the grid current was minimized. There was a difference in the amplitudes of the 3-phase currents due to a small negative q -axis current, as shown in the circled peaks. The validity of the proposed controller was presented clearly when the generator torque, stator reactive power, stator currents, and grid current ripples were controlled and reduced.

From the aforementioned results, it is evident that the synchronization process was achieved smoothly and without causing any disturbances in the grid voltage by using the proposed control scheme. In addition, the generator's 120 Hz torque oscillation component was suppressed significantly, while the 240 Hz and 360 Hz components were canceled by regulating the negative sequence of the rotor dq -axes currents. As a result, the torque oscillations of the DFIG were reduced from 2 Nm to only 0.3 Nm, which indicates the robustness and effectiveness of the proposed control method. Furthermore, it is well noted that the suggested torque elimination technique was effective in terms of reducing the stator reactive power ripples. Finally, the grid current ripple component was suppressed by controlling the negative component of the grid current.

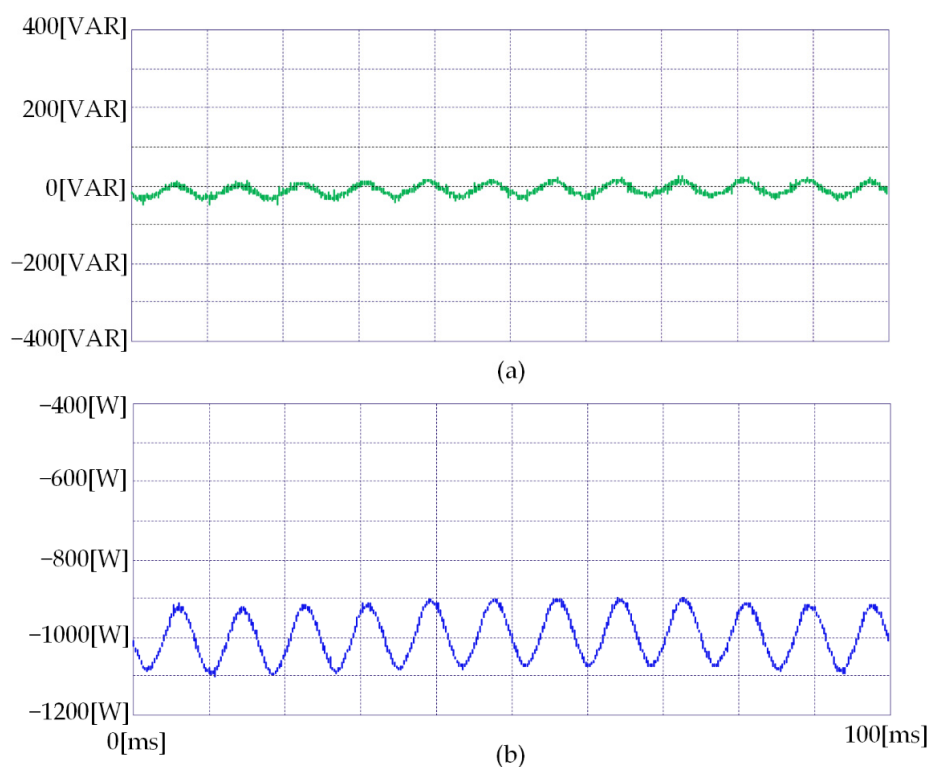


Figure 19. Steady-state stator (a) reactive power and (b) active power with torque ripple control.

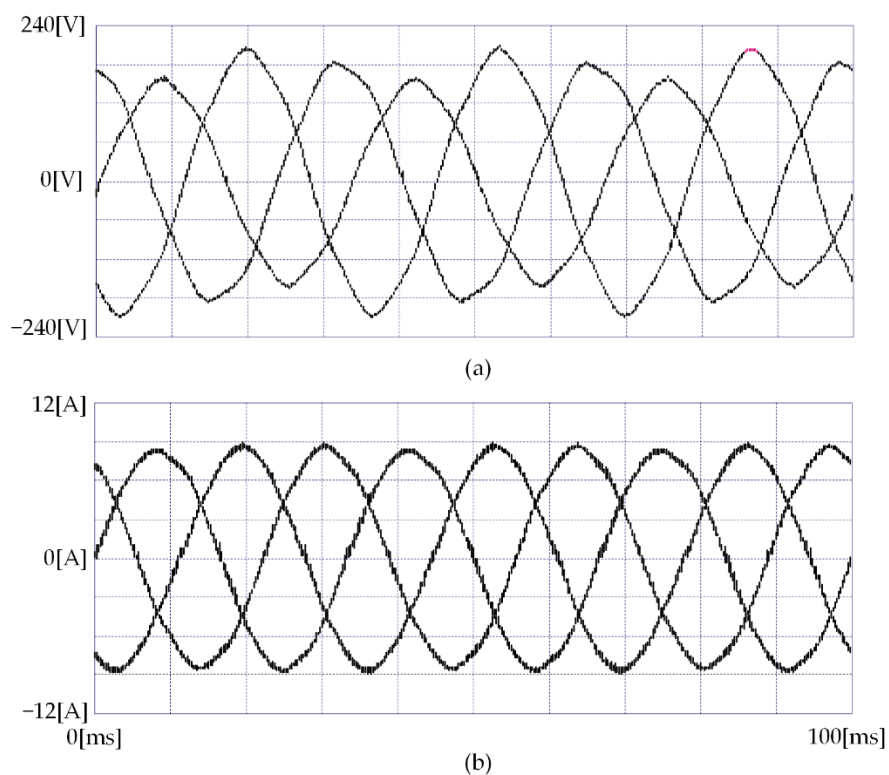


Figure 20. Steady-state (a) grid voltage and (b) controlled grid current.

7. Conclusions

This paper presented a coupling of a grid scheme for DFIG-based wind turbines under grid voltage imbalance conditions. The complete system design and control were implemented experimentally and the implementation methodology was presented. The

proposed controller was validated in the laboratory with a 3 kW system. The results of implementing the proposed algorithm were presented and discussed in the discussion section for symmetrical grid voltage imbalance during synchronization and operational conditions. The implementation of PI controllers to control the positive components of the rotor currents and PR controllers to control the negative sequence components of the rotor currents minimized the generator's torque ripples. At the same time, the stator reactive power ripple was also reduced significantly. The stator active power ripple, on the other hand, stayed similar to that generated by the standard control technique. Finally, the validity of the suggested method guaranteed smooth and fast synchronization and torque ripple elimination. During the start-up process, the proposed algorithm took about one cycle to adjust the generator EMF to the q -axis component of the grid voltage. The proposed structure and applied algorithm control of the positive and negative components of the rotor current significantly improved basic control performance, particularly when grid voltage imbalance was investigated.

Author Contributions: Conceptualization, A.G.A.-K. and T.S.; methodology, A.G.A.-K.; validation, A.S., M.A. and A.M.; formal analysis, A.S.; investigation, A.G.A.-K.; resources, M.A.; data curation, D.L. and A.M.; writing—original draft preparation, A.G.A.-K.; writing—review and editing, A.S.; visualization, T.S.; supervision, D.L. and A.M.; project administration, T.S.; funding acquisition, M.A. All authors have read and agreed to the published version of the manuscript.

Funding: This research received no external funding.

Institutional Review Board Statement: Not applicable.

Informed Consent Statement: Not applicable.

Data Availability Statement: Data are available within the article.

Acknowledgments: Ahmed Sobhy was funded by a scholarship (CSC number 2017GBJ001656) under the joint executive program between the Arab Republic of Egypt and China. Ahmed G. Abo-Khalil would like to thank the Deanship of Scientific Research at Majmaah University for supporting this work under project number 1440-31.

Conflicts of Interest: The authors declare no conflict of interest.

Nomenclature

ρ	Air density
ω_e	Angular velocity
R	Blade radius
λ	Blade tip speed ratio
T_e	Electromagnetic torque
e_{dqg}^p	Positive components of grid dq -axes voltages
e_{dqg}^n	Negative components of grid dq -axes voltages
L_m	Magnetizing inductance
i_{ms}	Magnetizing current
$C_p(\lambda, \beta)$	Power coefficient
B	Pitch angle
R_r	Rotor resistance
ω_r	Rotor angular velocity
v_{dqr}	Rotor dq -axes voltages
i_{dqr}	Rotor dq -axes currents
λ_{dqr}	Rotor dq -axes flux linkage
L_r	Rotor inductance
i_{dqr}^p	Positive components of rotor dq -axes currents
i_{dqr}^n	Negative components of rotor dq -axes currents

i_{dqr}^{n*}	Negative components of rotor dq -axes reference currents
R_s	Stator resistance
ω_{sl}	Slip angular velocity
v_{dqs}	Stator dq -axes voltages
i_{dqs}	Stator dq -axes currents
λ_{dqs}	Stator dq -axes flux linkage
P_s	Stator active power
Q_s	Stator reactive power
L_s	Stator inductance
v_{dqs}^p	Positive components of stator dq -axes voltages
i_{dqs}^p	Positive components of stator dq -axes currents
v_{dqs}^n	Negative components of stator dq -axes voltages
i_{dqs}^n	Negative components of stator dq -axes currents
λ_{dqs}^n	Negative components of stator dq -axes flux linkage
P_{s0}	Average component of the stator active power
Q_{s0}	Average component of the stator reactive power
T_{e0}	Average component of the electromagnetic torque
P_{esin2}	Sin oscillating stator power component at twice the grid frequency
P_{ecos2}	Cos oscillating stator power component at twice the grid frequency
Q_{esin2}	Sin oscillating stator reactive power component at twice the grid frequency
P_{ecos2}	Cos oscillating grid reactive power component at twice the grid frequency
T_{esin2}	Sin oscillating torque component at twice the grid frequency
T_{ecos2}	Cos oscillating torque component at twice the grid frequency
v	Wind speed
*	A superscript refers to the reference value of the variable

Appendix A

The specifications for the induction machine that was used for testing were as follows: three-phase, four poles, 230 V, 50 Hz, and 3 kW.

Table A1. Parameters of the turbine blade model.

Parameters	Value
Blade radius	1 m
Max. power conv. coefficient	0.42
Optimal tip speed ratio	8
Cut-in speed	4.5 m/s
Rated wind speed	13.5 m/s

Table A2. Parameters of the 3 kW doubly-fed induction generator.

Parameters	Value
Stator resistance	0.65 Ω
Rotor resistance	0.8 Ω
Iron loss resistance	155 Ω
Stator leakage inductance	0.003 H
Rotor leakage inductance	0.07 H
Mutual inductance	0.07 H

References

1. Ahmad, M. *Operation and Control of Renewable Energy Systems*; John Wiley & Sons: Chennai, India, 2018.
2. Lee, J.; Zhao, F. *Global Wind Report 2021*; GWEC: Brussels, Belgium, 2021.
3. Xu, D.; Blaabjerg, F.; Chen, W.; Zhu, N. *Advanced Control of Doubly Fed Induction Generator for Wind Power Systems*; John Wiley & Sons: Hoboken, NJ, USA, 2018.
4. Eltamaly, A.M.; Al-Saud, M.; Sayed, K.; Abo-Khalil, A.G. Sensorless Active and Reactive Control for DFIG Wind Turbines Using Opposition-Based Learning Technique. *Sustainability* **2020**, *12*, 3583. [[CrossRef](#)]

5. Tapia, G.; Santamaría, G.; Telleria, M.; Susperregui, A. Methodology for Smooth Connection of Doubly Fed Induction Generators to the Grid. *IEEE Trans. Energy Convers.* **2009**, *24*, 959–971. [[CrossRef](#)]
6. Abo-Khalil, A.G. Synchronization of DFIG output voltage to utility grid in wind power system. *Renew. Energy* **2012**, *44*, 193–198. [[CrossRef](#)]
7. Abdelbaset, A.; El-Sayed, A.M.; Abozeid, A.E.H. Grid synchronisation enhancement of a wind driven DFIG using adaptive sliding mode control. *IET Renew. Power Gener.* **2017**, *11*, 688–695. [[CrossRef](#)]
8. Xiong, L.; Li, P.; Wu, F.; Ma, M.; Khan, M.W.; Wang, J. A coordinated high-order sliding mode control of DFIG wind turbine for power optimization and grid synchronization. *Int. J. Electr. Power Energy Syst.* **2019**, *105*, 679–689. [[CrossRef](#)]
9. Elizondo, J.L.; Olloqui, A.; Rivera, M.; Macias, M.E.; Probst, O.; Micheloud, O.M.; Rodriguez, J. Model-Based Predictive Rotor Current Control for Grid Synchronization of a DFIG Driven by an Indirect Matrix Converter. *IEEE J. Emerg. Sel. Top. Power Electron.* **2014**, *2*, 715–726. [[CrossRef](#)]
10. Abo-Khalil, A.G.; Alghamdi, A.; Tlili, I.; Eltamaly, A.M. Current controller design for DFIG-based wind turbines using state feedback control. *IET Renew. Power Gener.* **2019**, *13*, 1938–1949. [[CrossRef](#)]
11. Abo-Khalil, A.G.; Alghamdi, A.S.; Eltamaly, A.M.; Al-Saud, M.S.; Praveen, R.P.; Sayed, K.; Bindu, G.R.; Tlili, I. Design of State Feedback Current Controller for Fast Synchronization of DFIG in Wind Power Generation Systems. *Energies* **2019**, *12*, 2427. [[CrossRef](#)]
12. Dida, A.; Merahi, F.; Mekhilef, S. New grid synchronization and power control scheme of doubly-fed induction generator based wind turbine system using fuzzy logic control. *Comput. Electr. Eng.* **2020**, *84*, 106647. [[CrossRef](#)]
13. Abo-Khalil, A.G.; Alharbi, W.; Al-Qawasmi, A.; Alobaid, M.; Alarifi, I. Modeling and control of unbalanced and distorted grid voltage of grid-connected DFIG wind turbine. *Int. Trans. Electr. Energy Syst.* **2021**, *31*, e12857. [[CrossRef](#)]
14. Qin, B.; Li, H.; Zhou, X.; Li, J.; Liu, W. Low-voltage ride-through techniques in DFIG-based wind turbines: A review. *Appl. Sci.* **2020**, *10*, 2154. [[CrossRef](#)]
15. Din, Z.; Zhang, J.; Xu, Z.; Zhang, Y.; Zhao, J. Low voltage and high voltage ride-through technologies for doubly fed induction generator system: Comprehensive review and future trends. *IET Renew. Power Gener.* **2021**, *15*, 614–630. [[CrossRef](#)]
16. Park, H.-G.; Abo-Khalil, A.G.; Lee, D.-C.; Son, K.-M. Torque Ripple Elimination for Doubly-Fed Induction Motors under Unbalanced Source Voltage. In Proceedings of the 7th International Conference on Power Electronics and Drive Systems, Bangkok, Thailand, 27–30 November 2007; pp. 1301–1306.
17. Zhou, Y.; Bauer, P.; Ferreira, J.A.; Pierik, J. Operation of Grid-Connected DFIG under Unbalanced Grid Voltage Condition. *IEEE Trans. Energy Convers.* **2009**, *24*, 240–246. [[CrossRef](#)]
18. Eltamaly, A.M.; Al-Saud, M.S.; Abo-Khalil, A.G. Dynamic Control of a DFIG Wind Power Generation System to Mitigate Unbalanced Grid Voltage. *IEEE Access* **2020**, *8*, 39091–39103. [[CrossRef](#)]
19. Kashkooli, M.R.A.; Madani, S.M.; Lipo, T.A. Improved Direct Torque Control for a DFIG under Symmetrical Voltage Dip with Transient Flux Damping. *IEEE Trans. Ind. Electron.* **2020**, *67*, 28–37. [[CrossRef](#)]
20. Shehata, E.G. Direct power control of wind-turbine-driven DFIG during transient grid voltage unbalance. *Wind Energy* **2014**, *17*, 1077–1091. [[CrossRef](#)]
21. Mazouz, F.; Belkacem, S.; Colak, I.; Drid, S.; Harbouche, Y. Adaptive direct power control for double fed induction generator used in wind turbine. *Int. J. Electr. Power Energy Syst.* **2020**, *114*, 105395–105405. [[CrossRef](#)]
22. Sahri, Y.; Tamalouzt, S.; Hamoudi, F.; Belaid, S.L.; Bajaj, M.; Alharthi, M.M.; Alzaidi, M.S.; Ghoneim, S.S.M. New intelligent direct power control of DFIG-based wind conversion system by using machine learning under variations of all operating and compensation modes. *Energy Rep.* **2021**, *7*, 6394–6412. [[CrossRef](#)]
23. Gao, S.; Mao, C.; Wang, D.; Lu, J. Dynamic performance improvement of DFIG-based WT using NADRC current regulators. *Int. J. Electr. Power Energy Syst.* **2016**, *82*, 363–372. [[CrossRef](#)]
24. Sobhy, A.; Lei, D. Model-assisted active disturbance rejection controller for maximum efficiency schemes of DFIG-based wind turbines. *Int. Trans. Electr. Energy Syst.* **2021**, *31*, e13107. [[CrossRef](#)]
25. Jaladi, K.K.; Sandhu, K.S. DC-link transient improvement of SMC-based hybrid control of DFIG-WES under asymmetrical grid faults. *Int. Trans. Electr. Energy Syst.* **2018**, *28*, 2633–2659. [[CrossRef](#)]
26. Han, Y.; Ma, R. Adaptive-Gain Second-Order Sliding Mode Direct Power Control for Wind-Turbine-Driven DFIG under Balanced and Unbalanced Grid Voltage. *Energies* **2019**, *12*, 3886. [[CrossRef](#)]
27. Cheng, C.; Cheng, P.; Nian, H.; Sun, D. Model predictive stator current control of doubly fed induction generator during network unbalance. *IET Power Electron.* **2018**, *11*, 120–128. [[CrossRef](#)]
28. Khan, I.; Zeb, K.; Din, W.U.; Islam, S.U.; Ishfaq, M.; Hussain, S.; Kim, H.-J. Dynamic Modeling and Robust Controllers Design for Doubly Fed Induction Generator-Based Wind Turbines under Unbalanced Grid Fault Conditions. *Energies* **2019**, *12*, 454. [[CrossRef](#)]
29. Hu, J.-B.; He, Y.-K.; Wang, H.-S. Adaptive rotor current control for wind-turbine driven DFIG using resonant controllers in a rotor rotating reference frame. *J. Zhejiang Univ. Sci. A* **2008**, *9*, 149–155. [[CrossRef](#)]
30. Hu, J.; He, Y.; Xu, L.; Williams, B.W. Improved Control of DFIG Systems during Network Unbalance Using PI-R Current Regulators. *IEEE Trans. Ind. Electron.* **2009**, *56*, 439–451. [[CrossRef](#)]
31. Phan, V.-T.; Lee, H.-H. Enhanced Proportional-Resonant Current Controller for Unbalanced Stand-alone DFIG-based Wind Turbines. *J. Electr. Eng. Technol.* **2010**, *5*, 443–450. [[CrossRef](#)]

32. Yan, Y.; Wang, M.; Song, Z.-F.; Xia, C.-L. Proportional-Resonant Control of Doubly-Fed Induction Generator Wind Turbines for Low-Voltage Ride-Through Enhancement. *Energies* **2012**, *5*, 4758–4778. [[CrossRef](#)]
33. Heier, S. *Grid Integration of Wind Energy: Onshore and Offshore Conversion Systems*, 3rd ed.; John Wiley & Sons: Chichester, UK, 2014.
34. Abo-Khalil, A.G.; Abo-Zied, H. Sensorless Control for DFIG Wind Turbines Based on Support Vector Regression. In Proceedings of the 38th Annual Conference on IEEE Industrial Electronics Society, Montreal, QC, Canada, 25–28 October 2012; pp. 3475–3492.
35. Abo-Khalil, A.G. Grid Connection Control of DFIG for Variable Speed Wind Turbines under Turbulent Conditions. *IJRER* **2019**, *9*, 1260–1271.
36. Khan, A.; Hu, X.M.; Khan, M.A.; Barendse, P. Doubly Fed Induction Generator Open Stator Synchronized Control during Unbalanced Grid Voltage Condition. *Energies* **2020**, *13*, 3155. [[CrossRef](#)]
37. Ozsoy, E.; Soner, B.; Ahmad, F.; Rasool, A.; Sabanovic, A.; Gokasan, M.; Bogosyan, S.; Sanjeevikumar, P. Disturbance Observer Based Power Control of DFIG under Unbalanced Network Conditions. *Electr. Power Compon. Syst.* **2018**, *46*, 1448–1461. [[CrossRef](#)]
38. López, A.R.; Mina, J.D.; Calderón, G.; Aguayo, J.; Calleja, J.H. Combined parameters selection of a proportional integral plus resonant controller for harmonics compensation in a wind energy conversion system. *Electr. Eng.* **2018**, *100*, 2277–2286. [[CrossRef](#)]